Strongly enhanced photoluminescence in nanostructured monolayer MoS_2 by chemical vapor deposition

2016 Nanotechnology 27 135706

(http://iopscience.iop.org/0957-4484/27/13/135706)

IOP Publishing Nanotechnology
Nanotechnology 27 (2016) 135706 (7pp) doi:10.1088/0957-4484/27/13/135706

Strongly enhanced photoluminescence in nanostructured monolayer MoS_2 by chemical vapor deposition

Yi Zhu[1], Jiong Yang[1], Shuang Zhang[1], Salman Mokhtar[1], Jiajie Pei[1,2], Xinghua Wang[1] and Yuerui Lu[1]

[1] Research School of Engineering, College of Engineering and Computer Science, The Australian National University, Canberra, ACT, 0200, Australia
[2] School of Mechanical Engineering, Beijing Institute of Technology, Beijing, 100081, People's Republic of China

E-mail: yuerui.lu@anu.edu.au

Received 16 December 2015, revised 21 January 2016
Accepted for publication 26 January 2016
Published 22 February 2016

Abstract

Two-dimensional (2D) layered molybdenum disulfide (MoS_2) has become a very promising candidate semiconducting material for future optoelectronic devices, owing to its unique properties. However, monolayer MoS_2 is still a weak photon emitter, compared with other direct band gap semiconductors, which requires extra techniques or complicated steps to enhance its photon emission efficiency. Here, we demonstrated that nanostructured monolayer MoS_2, produced by one-step chemical vapor deposition (CVD) growth, shows highly enhanced PL emission. The effective enhancement factor could be up to ~43. Our results open the door to manipulating the optical properties of future devices by using nanostructured 2D monolayers.

S Online supplementary data available from stacks.iop.org/NANO/27/135706/mmedia

Keywords: MoS_2, photoluminescence enhancement, 2D, edge states

Due to their highly active edge sites, molybdenum disulfide (MoS_2) nanomaterials have shown exceptionally promising applications in various fields, including nanotribology [1], photocatalysis [2], the hydrodesulphurization (HDS) process [3], hydrogen evolution reaction (HER) catalysis [4, 5], saturable absorption in ultra-fast photonics [6, 7] and solar cells [8]. Recently emerging two-dimensional (2D) atomically thin MoS_2 materials have also attracted extensive investigations [9–16], due to their great potential applications for future electronic and optoelectronic devices, like field effect transistors, light emitting devices, photodetectors, etc. MoS_2 is very stable in ambient conditions, which is in great contrast to other unstable 2D semiconductors like black phosphorus [17–21], $MoTe_2$ [22, 23], etc. The band gap nature of MoS_2 changes from indirect to direct as the layer number is thinned down to a monolayer [13], which leads to extraordinary photoluminescence (PL) and strongly enhanced optoelectronic responses in monolayer MoS_2. However, the PL of monolayer MoS_2 is still weaker than we would expect for a high-quality direct band gap emitter, mainly because of the intrinsic defects and heavy intrinsic n-type doping in monolayer MoS_2 [12]. Various techniques have been reported to enhance the PL efficiency of monolayer MoS_2, such as carrier density engineering via electrical static gating and chemical doping [24–26], absorption enhancement through plasmonic nanostructures [27, 28] and defect engineering by plasma irradiation [29–31]. All those methods require extra fabrication steps, which potentially increases the cost. Here, we demonstrated that nanostructured monolayer MoS_2 produced by one-step chemical vapor deposition (CVD) growth shows highly enhanced PL emission, compared with large-size monolayer MoS_2 samples prepared by mechanical exfoliation [32] and CVD growth [33–36]. The PL enhancement is mainly due to the large amount of edge states associated with the nanostructured MoS_2. This type of edge states induced PL enhancement was also observed in CVD-grown WS_2 flakes [37]. Our method opens the door for high-performance optoelectronic devices based on nanostructured monolayer

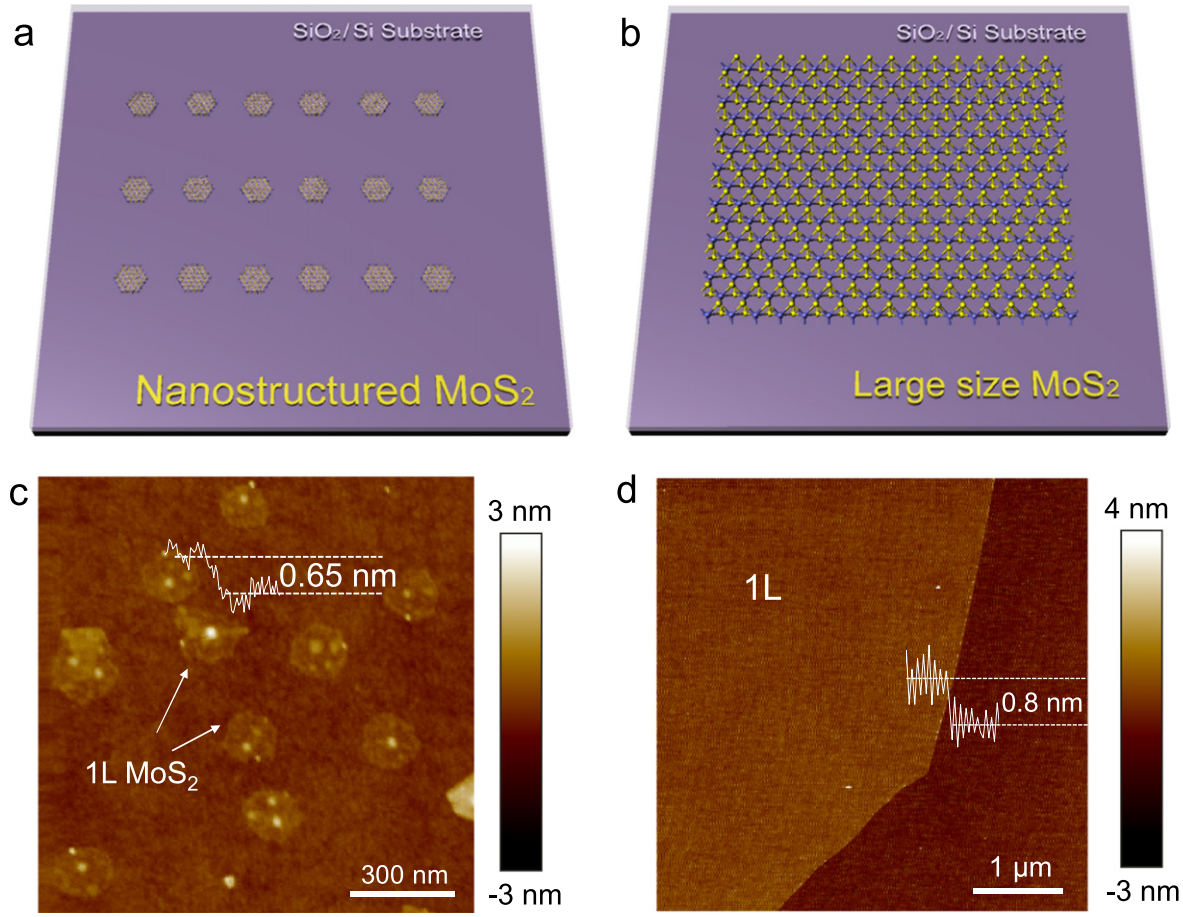

Figure 1. Schematic and AFM images of nanostructured monolayer MoS_2 and large-size monolayer MoS_2. (a) Schematic of nanostructured monolayer MoS_2 synthesized by chemical vapor deposition. The MoS_2 flakes are randomly distributed upon a SiO_2/Si substrate with quasi-hexagonal shape. (b) Schematic of large-size monolayer MoS_2 obtained by mechanical exfoliation. (c) Atomic force microscopy (AFM) image of nanostructured monolayer MoS_2 with thickness of 0.65 nm. (d) AFM image of exfoliated monolayer MoS_2 flake with thickness of 0.8 nm.

MoS_2. Besides, since the nanostructured MoS_2 flakes are small in size, they could be dispersed in liquid-like liquid crystal to make them as a module of optoelectronic devices [38]. Furthermore, nanostructured MoS_2 flakes could also possibly serve as nanocatalysts owing to their highly enhanced surface area [4].

Here, we aim to fabricate nanostructured monolayer MoS_2 using CVD, which has a large amount of edge states for PL enhancement (figure 1). The growth condition for nanostructured monolayer MoS_2 is slightly different from that for large-size monolayer MoS_2 growth. The main difference is that we used two steps in the growth process. During the first step, a MoO_3 source was thermally evaporated quickly and was deposited on a substrate to form plenty of nucleate sites on the substrate. A large quantity of these nucleate centers offered a good condition to form nanostructured monolayer MoS_2, since molecules tended to bond into nucleate centers rather than the edge of the MoS_2 surface. In the second step, we quickly introduced sulphur powder to the 150 °C temperature zone, by using a magnetically controlled set-up. A vast amount of sulphur vapor was introduced and the increased sulphur partial pressure resulted in the formation of nanostructured MoS_2. The grown MoS_2 nano-disk monolayer showed quasi-hexagonal shape and a size ~100 nm and these nano-plates were randomly distributed on the SiO_2/Si substrate (figures 1(a) &(c)). The monolayer thickness was confirmed by atomic force microscopy (AFM) height analysis (figure 1(c)).

The optical properties were studied by micro-Raman and PL spectroscopy with a 532 nm laser as the excitation. The nanostructured monolayer MoS_2 sample shows two strong Raman peaks at 384 and 404 cm^{-1} (figure 2(a)), which correspond to the in-plane E^1_{2g} and out-plane A_{1g} of monolayer MoS_2, respectively [39]. The Raman spectrum of our nanostructured monolayer MoS_2 is comparable with those of large-size MoS_2, which are also shown in figure 2(a). The Raman peak at ~456 cm^{-1} involves two longitudinal acoustic phonons (2LA(M)) arising from the edge of the Brillouin zone (BZ) [40, 41]. Besides the nanostructured monolayer MoS_2, we also fabricated large-size monolayer MoS_2 samples by CVD (see supplementary information) and one large-size 1L MoS_2 by mechanical exfoliation (figure 1(d)) as the control samples. The exfoliated MoS_2 sample has a PL peak at ~1.83 eV (trion peak of MoS_2), which is due to the intrinsic

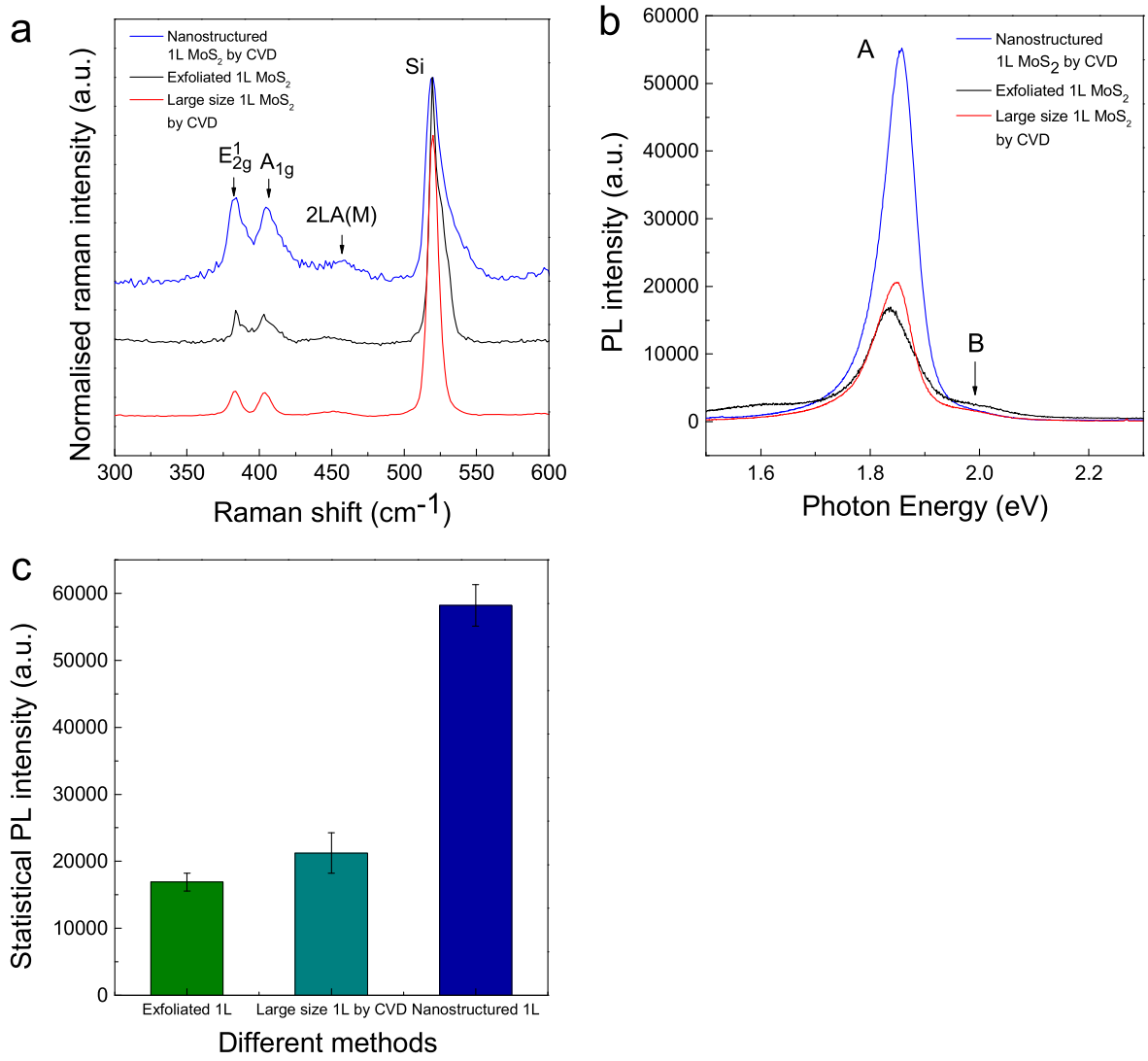

Figure 2. Strongly enhanced photoluminescence (PL) in nanostructured monolayer MoS_2. (a) Raman spectrum of nanostructured monolayer MoS_2 and 1L large-size MoS_2 (exfoliated and grown by CVD). (b) PL spectrum of CVD-grown nanostructured monolayer MoS_2, one-layer MoS_2 flake produced by mechanical exfoliation and large-size one-layer MoS_2 by CVD growth. (c) The statistical PL intensity values for exfoliated, large-size CVD monolayer and nanostructured CVD monolayer MoS_2 samples, under the same excitation condition. At least three batches of exfoliated, large-size CVD monolayer MoS_2 and nanostructured CVD monolayer MoS_2 samples were characterized to get statistical data.

n-type doping in the exfoliated MoS_2 samples [26]; on the other hand, the nanostructured CVD monolayer MoS_2 (figure 2(b)) and the large-size monolayer CVD MoS_2 samples have a PL peak at ~1.87 eV (neutral exciton peak of MoS_2), which indicates that both of those two CVD samples have a low or even comparable initial doping level. The energy difference between trions and excitons in our experiment is compatible with previous results [26]. This also proves that the nanostructured monolayer MoS_2 possesses the same energy band gap as the large-size monolayer MoS_2 samples. The large-size monolayer MoS_2 by CVD shows comparable PL intensity with the exfoliated monolayer MoS_2, which is consistent with previous reports [34, 35]. But interestingly, the PL intensity from the nanostructured monolayer MoS_2 was around 3.5 times higher than those from the large-size CVD monolayer MoS_2 and exfoliated monolayer MoS_2 samples (figure 2(b)). In experiments, we fabricated at least three batches of CVD monolayers, exfoliated MoS_2 monolayers and nanostructured monolayer MoS_2 samples to obtain statistical PL intensity values. The nanostructured MoS_2 monolayers showed an average PL enhancement factor of ~3.4, compared with the CVD large-size monolayers (figure 2(c)). Considering the fact that the area filling ratio of the nanostructured MoS_2 is only ~7%, the PL enhancement factor normalized to the area size is up to ~43. We have also calculated the filling ratios and enhancement factors of the five conditions presented in figure 2(c) (see supplementary information). Considering the relatively low initial doping level in both our nanostructured and large-size monolayer MoS_2 samples, the doping level difference in our samples could not explain the large PL enhancement factor up to ~43. On the other hand, this large PL

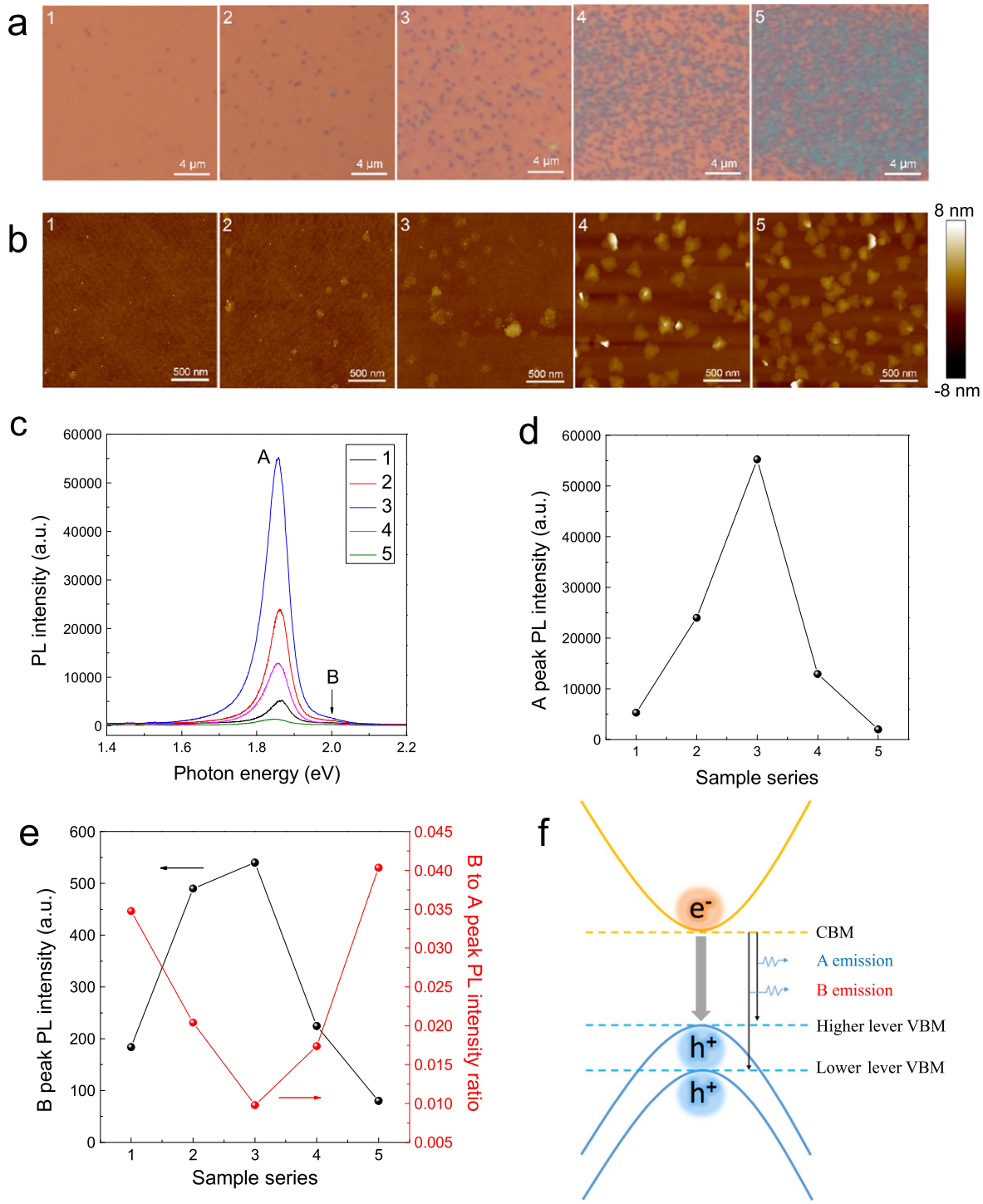

Figure 3. Density-dependent PL enhancement in nanostructured MoS_2. (a) Microscope image of five chips with different density of nanostructured MoS_2. The density is gradually increased from chip 1 to chip 5. (b) AFM images of the nanostructured MoS_2 from chips 1–5, respectively. (c) Measured PL spectra from chips 1–5. (d) The maximum A peak intensity of the PL spectrum in (c). (e) The maximum B peak intensity of the PL spectrum in (c) and maximum PL intensity ratio of B peak to A peak. (f) Schematic presents the valence-band spin-orbit splitting of the direct gap transition at the K point and A, B emission peak, where CBM is conduction band minimum and VBM is valence band maximum.

enhancement in the nanostructured monolayer MoS_2 samples could be due to their large amount of edge states, which were also observed in CVD-grown WS_2 flakes [37]. Another small peak at ~2.03 eV (B peak) in the PL spectrum corresponds to the valence-band spin-orbit splitting of the direct gap transition at the K point [32]. Interestingly, the intensity of the B peak in the nanostructured 1L MoS_2 is lower than that in the exfoliated monolayer MoS_2 sample (discussed later).

In experiments, we found that the morphology of the nanostructured MoS_2 was very sensitive to the local growth

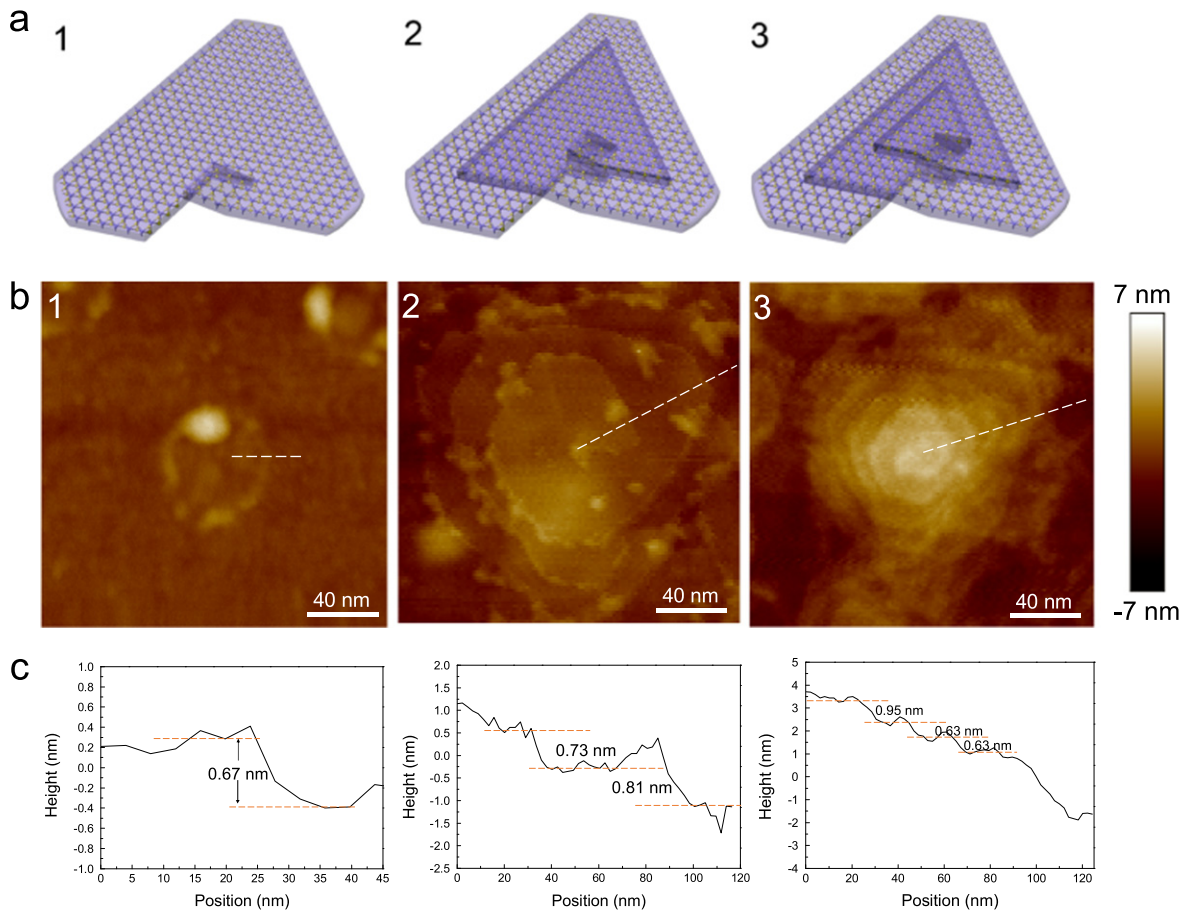

Figure 4. Evolution of MoS_2 nanostructured monolayer to a multilayer spiral 3D structure. (a) Schematic of monolayer growing into multilayer spiral MoS_2. Image 1 is the first stage of forming a monolayer MoS_2 flake. Image 2 shows spiral growth from a monolayer to a three-layer structure. Image 3 is of multilayer spiral pyramid-shaped MoS_2. (b) AFM images of different MoS_2 structures corresponding to these three stages indicated in (a). (c) Height profile of the corresponding region (indicated by dashed lines) in (b).

conditions, such as the density of the nuclear seeds and also the pressure of the sulphur gas. We probed five chips that were placed at different locations of the furnace as shown in figure 3, with chip 1 close to the edge and chip 5 close to the center of the tube. At locations closer to the tube center, higher densities of nuclear sites were deposited, which led to much higher densities of MoS_2 flakes (figures 3(a) & (b)). The density of the MoS_2 flakes gradually increased from chip 1 to chip 5; however, the PL intensity increased from chip 1 to chip 3 and then decreased gradually from chip 3 to chip 5 (figure 3(c)). This evolution can be understood from the morphology of the nanostructured MoS_2 flakes. From the AFM images (figure 3(b)), the density of monolayer MoS_2 nano-plates increased from location 1 to location 3, which leads to the increasing of the PL intensity. In chips 4 and 5, multilayer MoS_2 nano-plates began to form and these multilayer MoS_2 flakes show an indirect band gap nature, leading to lower PL emission efficiency [32] (figures 3(c) & (d)). The prominent PL peaks of these five chips are all located at ~1.87 eV (a peak from neutral excitons of MoS_2). In addition, we also recorded the PL intensity of the B peak from each location and compared the intensity ratio of the B peak to the A peak (figure 3(e)). Although B peak intensity showed the same trend as for the A peak, the B/A intensity ratio decreased first then began to increase, suggesting a totally opposite trend compared with the trend of A peak intensity. This means that the nanostructured monolayer MoS_2 can enhance the PL emission at the A peak on the one hand, but suppress the emission at the B peak on the other hand. The B peak arises from the direct gap transition between the minima of the conduction band and the lower-level valence-band maxima that is created by valence-band spin-orbit splitting at the K point (figure 3(f)) [42]. The suppression of the emission at the B peak could be because of the enhancement of PL emission at lower-energy emission at the A peak, since the total amount of photo-excited carriers is limited to a constant number.

In order to better understand the decrease of the PL intensity from chip 3 to chip 5, we investigated the mechanism for the formation of multilayer MoS_2 nano-plates. Interestingly, we found that the multilayer MoS_2 nano-plates have 3D spiral pyramid structures. During our CVD growth, the relatively high sulphur pressure resulted in screw dislocation in the monolayer MoS_2 nano-plates, which leads to

the formation of a spiral MoS_2 structure, similar to a previous report [43]. Figure 4(a) shows schematics of each stage in figure 4(b). As we can see from the left image of figure 4(b), some atomic clusters formed on the substrate and began to grow up, forming one monolayer MoS_2 nano-plate. At the same time, we also noticed that there was one bright spot on the edge of the monolayer MoS_2 nano-plate, which was identified as screw dislocation. The incoming molecules tend to combine with these dislocations to decrease the total surface energy [44]. As the nano-plate grows up, the bottom layer keeps extending. Meanwhile, the upper layer also absorbs molecules then grows along with the screw dislocations and forms a bilayer (middle image of figure 4(b)). The top area is always smaller than the bottom layer due to different growth times. This results in a net trend of vertical growth and the formation of a multilayer pyramid structure (right image of figure 4(b)). Those multilayer pyramid MoS_2 nano-plates have an indirect band gap nature, similar to multilayer MoS_2, leading to the decrease of PL intensity in chips 4 and 5.

Conclusions

In conclusion, we have demonstrated that CVD-grown nanostructured monolayer MoS_2 shows strongly enhanced efficiency of photon emission, because of the large amount of edge states. The effective enhancement factor was measured to be up to ~43. Meanwhile, we showed that the formation of the 3D spiral pyramid MoS_2 was the reason preventing the further enhancement of PL from these nanostructured MoS_2 samples.

Experiment

Methods

Growth of monolayer and multilayer MoS_2. Our MoS_2 sample was prepared by using ambient CVD with MoO_3 and sulphur powder as precursors. The substrate was placed face down onto MoO_3 above one quartz sample boat. The boat contained 5 mg MoO_3 (⩾99.5%, sigma-Aldrich) and was put into the center of a furnace. Another boat containing 200 mg S (⩾99.5%, sigma-Aldrich) was placed into a tube but outside the furnace. The system was washed by nitrogen gas with 200 sccm flow rate for 1 h and then ramped up to 700 °C in 30 min. When the temperature went up to 600 °C, the S powder was inserted. At this moment, the temperature for the S powder was 150 °C and then the flow rate was changed from 200 sccm to 50 sccm, to sit for 8 min at 700 °C. Finally it was cooled down to room temperature with 200 sccm N_2. Although some different morphologies of MoS_2 showed up, the major morphology in each chip at different locations in each batch is consistent. Also, the PL properties are similar in the same distribution area.

Sample characterization

AFM measurement was carried out with a Bruker Multi-Mode III AFM. All PL and Raman measurements were run by a T64000 micro-Raman system and the laser spot has a spatial resolution of sub-1 μm.

References

[1] Chhowalla M and Amaratunga G A J 2000 Thin films of fullerene-like MoS_2 nanoparticles with ultra-low friction and wear *Nature* **407** 164–7

[2] Wilcoxon J P, Thurston T R and Martin J E 1999 Applications of metal and semiconductor nanoclusters as thermal and photo-catalysts *Nanostruct. Mater.* **12** 993–7

[3] Paul J-F and Payen E 2003 Vacancy formation on MoS_2 hydrodesulfurization catalyst: DFT study of the mechanism *J. Phys. Chem.* B **107** 4057–64

[4] Jaramillo T F, Jørgensen K P, Bonde J, Nielsen J H, Horch S and Chorkendorff I 2007 Identification of active edge sites for electrochemical H_2 evolution from MoS_2 nanocatalysts *Science* **317** 100–2

[5] Chen Z, Cummins D, Reinecke B N, Clark E, Sunkara M K and Jaramillo T F 2011 Core–shell MoO_3–MoS_2 nanowires for hydrogen evolution: a functional design for electrocatalytic materials *Nano Lett.* **11** 4168–75

[6] Du J, Wang Q, Jiang G, Xu C, Zhao C, Xiang Y, Chen Y, Wen S and Zhang H 2014 Ytterbium-doped fiber laser passively mode locked by few-layer Molybdenum Disulfide (MoS_2) saturable absorber functioned with evanescent field interaction *Sci. Rep.* **4** 6346

[7] Zhang H, Lu S B, Zheng J, Du J, Wen S C, Tang D Y and Loh K P 2014 Molybdenum disulfide (MoS(2)) as a broadband saturable absorber for ultra-fast photonics *Opt. Express* **22** 7249–60

[8] Gourmelon E, Lignier O, Hadouda H, Couturier G, Bernède J C, Tedd J, Pouzet J and Salardenne J 1997 MS_2 (M = W, Mo) photosensitive thin films for solar cells *Sol. Energy Mater. Sol. Cells* **46** 115–21

[9] Bertolazzi S, Brivio J and Kis A 2011 Stretching and breaking of ultrathin MoS_2 *ACS Nano* **5** 9703–9

[10] Lee C, Yan H, Brus L E, Heinz T F, Hone J and Ryu S 2010 Anomalous lattice vibrations of single- and few-layer MoS_2 *ACS Nano* **4** 2695–700

[11] Li Y, Rao Y, Mak K F, You Y, Wang S, Dean C R and Heinz T F 2013 Probing symmetry properties of few-layer MoS_2 and h-BN by optical second-harmonic generation *Nano Lett.* **13** 3329–33

[12] Mak K F, He K, Lee C, Lee G H, Hone J, Heinz T F and Shan J 2013 Tightly bound trions in monolayer MoS_2 *Nat. Mater.* **12** 207–11

[13] Mak K F, Lee C, Hone J, Shan J and Heinz T F 2010 Atomically thin MoS_2: a new direct-gap semiconductor *Phys. Rev. Lett.* **105** 136805

[14] Zeng H, Dai J, Yao W, Xiao D and Cui X 2012 Valley polarization in MoS_2 monolayers by optical pumping *Nat. Nanotechnol.* **7** 490–3

[15] Yang J *et al* 2014 Atomically thin optical lenses and gratings arXiv:1411

[16] Pei J *et al* 2015 Exciton and trion dynamics in bilayer MoS_2 *Small* **11** 6384–90

[17] Li L, Yu Y, Ye G J, Ge Q, Ou X, Wu H, Feng D, Chen X H and Zhang Y 2014 Black phosphorus field-effect transistors *Nat. Nanotechnol.* **9** 372–7
[18] Xu R, Yang J, Zhu Y, Yan H, Pei J, Myint Y W, Zhang S and Lu Y 2016 Layer-dependent surface potential of phosphorene and anisotropic/layer-dependent charge transfer in phosphorene-gold hybrid systems *Nanoscale* **8** 129–35
[19] Yang J, Xu R, Pei J, Myint Y W, Wang F, Wang Z, Zhang S, Yu Z and Lu Y 2015 Optical tuning of exciton and trion emissions in monolayer phosphorene *Light Sci. Appl.* **4** e312
[20] Xu R *et al* 2015 Extraordinarily bound quasi-one-dimensional trions in two-dimensional phosphorene atomic semiconductors *ACS Nano* (doi:10.1021/acsnano.5b06193)
[21] Zhang S *et al* 2014 Extraordinary photoluminescence and strong temperature/angle-dependent Raman responses in few-layer phosphorene *ACS Nano* **8** 9590–6
[22] Yang J, Lü T, Myint Y W, Pei J, Macdonald D, Zheng J-C and Lu Y 2015 Robust excitons and trions in monolayer $MoTe_2$ *ACS Nano* **9** 6603–9
[23] Ruppert C, Aslan O B and Heinz T F 2014 Optical properties and band gap of single- and few-layer $MoTe_2$ crystals *Nano Lett.* **14** 6231–6
[24] Newaz A K M, Prasai D, Ziegler J I, Caudel D, Robinson S, Haglund R F Jr and Bolotin K I 2013 Electrical control of optical properties of monolayer MoS_2 *Solid State Commun.* **155** 49–52
[25] Tongay S, Zhou J, Ataca C, Liu J, Kang J S, Matthews T S, You L, Li J, Grossman J C and Wu J 2013 Broad-range modulation of light emission in two-dimensional semiconductors by molecular physisorption gating *Nano Lett.* **13** 2831–6
[26] Mouri S, Miyauchi Y and Matsuda K 2013 Tunable photoluminescence of monolayer MoS_2 via chemical doping *Nano Lett.* **13** 5944–8
[27] Butun S, Tongay S and Aydin K 2015 Enhanced light emission from large-area monolayer MoS_2 using plasmonic nanodisc arrays *Nano Lett.* **15** 2700–4
[28] Lee B, Park J, Han G H, Ee H-S, Naylor C H, Liu W, Johnson A T C and Agarwal R 2015 Fano resonance and spectrally modified photoluminescence enhancement in monolayer MoS_2 integrated with plasmonic nanoantenna array *Nano Lett.* **15** 3646–53
[29] Komsa H-P, Kotakoski J, Kurasch S, Lehtinen O, Kaiser U and Krasheninnikov A V 2012 Two-dimensional transition metal dichalcogenides under electron irradiation: defect production and doping *Phys. Rev. Lett.* **109** 035503
[30] Tongay S *et al* 2013 Defects activated photoluminescence in two-dimensional semiconductors: interplay between bound, charged, and free excitons *Sci. Rep.* **3** 2657
[31] Nan H *et al* 2014 Strong photoluminescence enhancement of MoS_2 through defect engineering and oxygen bonding *ACS Nano* **8** 5738–45
[32] Splendiani A, Sun L, Zhang Y, Li T, Kim J, Chim C-Y, Galli G and Wang F 2010 Emerging photoluminescence in monolayer MoS_2 *Nano Lett.* **10** 1271–5
[33] Lee Y-H *et al* 2012 Synthesis of large-area MoS_2 atomic layers with chemical vapor deposition *Adv. Mater.* **24** 2320–5
[34] Jeon J, Jang S K, Jeon S M, Yoo G, Jang Y H, Park J-H and Lee S 2015 Layer-controlled CVD growth of large-area two-dimensional MoS_2 films *Nanoscale* **7** 1688–95
[35] Chen C, Qiao H, Xue Y, Yu W, Song J, Lu Y, Li S and Bao Q 2015 Growth of large-area atomically thin MoS_2 film via ambient pressure chemical vapor deposition *Photonics Res.* **3** 110–4
[36] Wang S, Rong Y, Fan Y, Pacios M, Bhaskaran H, He K and Warner J H 2014 Shape evolution of monolayer MoS_2 crystals grown by chemical vapor deposition *Chem. Mater.* **26** 6371–9
[37] Gutiérrez H R, Perea-López N, Elías A L, Berkdemir A, Wang B, Lv R, López-Urías F, Crespi V H, Terrones H and Terrones M 2013 Extraordinary room-temperature photoluminescence in triangular WS_2 monolayers *Nano Lett.* **13** 3447–54
[38] Cao W J, Wang H Y, Luo A P, Luo Z C and Xu W C 2012 Graphene-based, 50 nm wide-band tunable passively Q-switched fiber laser *Laser Phys. Lett.* **9** 54–8
[39] Liang L and Meunier V 2014 First-principles Raman spectra of MoS_2, WS_2 and their heterostructures *Nanoscale* **6** 5394–401
[40] Gołasa K, Grzeszczyk M, Binder J, Bożek R, Wysmołek A and Babiński A 2015 The disorder-induced Raman scattering in Au/MoS_2 heterostructures *AIP Adv.* **5** 077120
[41] Gołasa K, Grzeszczyk M, Leszczyński P, Faugeras C, Nicolet A A L, Wysmołek A, Potemski M and Babiński A 2014 Multiphonon resonant Raman scattering in MoS_2 *Appl. Phys. Lett.* **104** 092106
[42] Coehoorn R, Haas C and de Groot R A 1987 Electronic structure of $MoSe_2$, MoS_2, and WSe_2: II. The nature of the optical band gaps *Phys. Rev.* B **35** 6203–6
[43] Zhang L, Liu K, Wong A B, Kim J, Hong X, Liu C, Cao T, Louie S G, Wang F and Yang P 2014 Three-dimensional spirals of atomic layered MoS_2 *Nano Lett.* **14** 6418–23
[44] Jin S, Bierman M J and Morin S A 2010 A new twist on nanowire formation: screw-dislocation-driven growth of nanowires and nanotubes *J. Phys. Chem. Lett.* **1** 1472–80

Supplementary Information for

Strongly Enhanced Photoluminescence in Nanostructured Monolayer MoS_2 by Chemical Vapor Deposition

Yi Zhu, [1] Jiong Yang, [1] Shuang Zhang, [1] Salman Mokhtar, [1] Jiajie Pei, [1, 2] Xinghua Wang, [1] and Yuerui Lu[1*]

[1]Research School of Engineering, College of Engineering and Computer Science, the Australian National University, Canberra, ACT, 0200, Australia

[2]School of Mechanical Engineering, Beijing Institute of Technology, Beijing, 100081, China

***** To whom correspondence should be addressed: Yuerui Lu (yuerui.lu@anu.edu.au)

1. Characterization of large-size monolayer MoS_2 by CVD

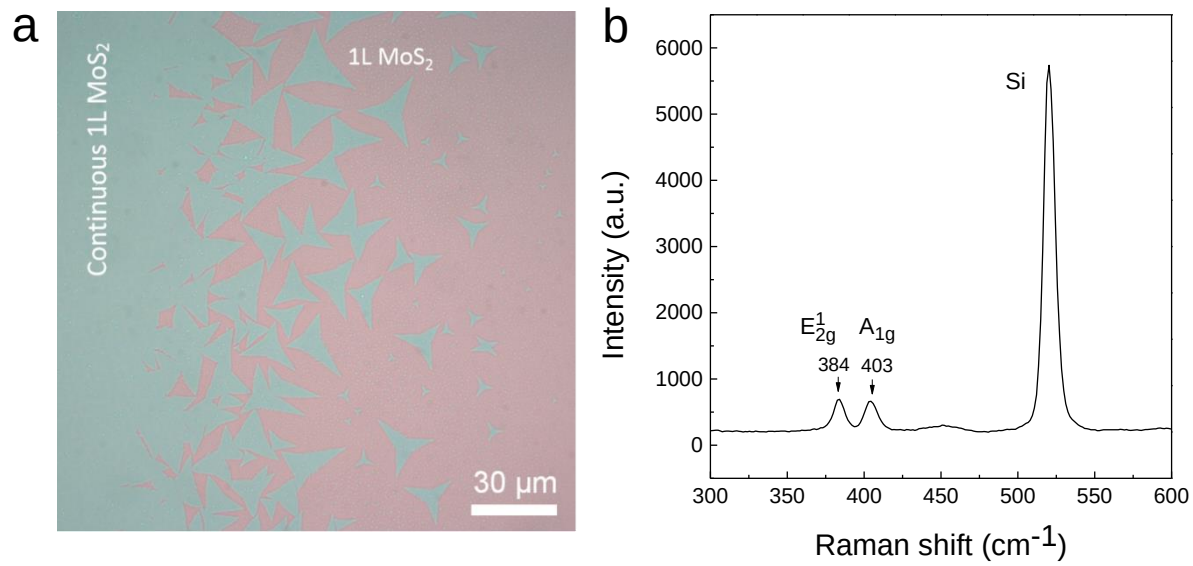

Figure S1 | Characterization of large-size monolayer MoS_2 by CVD. a, Optical microscope image of monolayer MoS_2 by using chemical vapour deposition method. The triangle shape areas are isolated 1L MoS_2, while the right large part is continuous 1L MoS_2 film. **b,** Raman spectrum of triangle shape 1L MoS_2 and it was measured in a confocal spectrometer with a 532 nm excitation laser.

2. CVD magnetically controlled set up

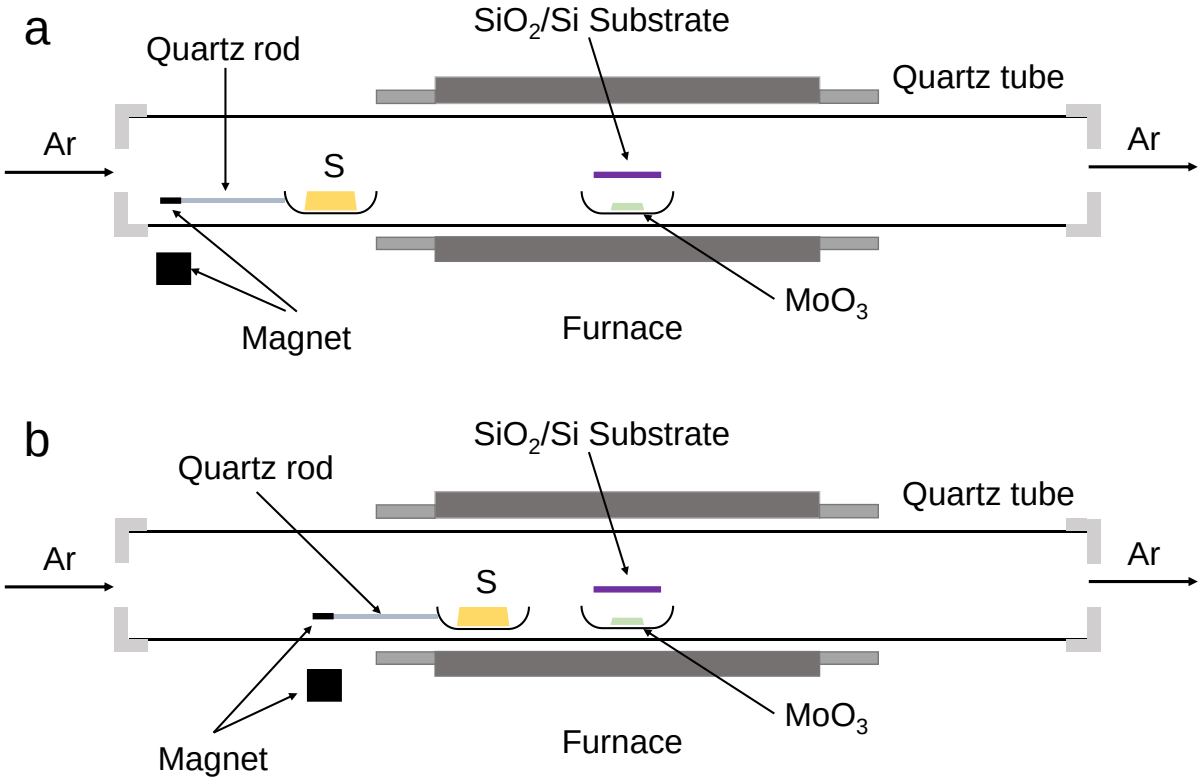

Figure S2 | CVD furnace and magnetically controlled set up. a, first step: MoO_3 source thermally evaporated and deposited onto substrate. **b,** second step: when furnace temperature ramp to 600 ℃, quickly inset S power by using magnetic force push evaporator boat into designed location.